Ventilation Control of Air Pollutant during Preventive Maintenance of a Metal Etcher in Semiconductor Industry

Chih-Liang Chien[1], Chuen-Jinn Tsai[1*], Kwen-wen Ku[1], Shou-Nan Li[2]

[1] *Institute of Environmental Engineering, National Chiao Tung University, No. 75 Poai St., Hsin Chu, Taiwan.*

[2] *Energy and Environment Research Laboratories, Industrial Technology Research Institute (ITRI), Hsinchu, Taiwan.*

ABSTRACT

Ventilation control efficiency of air pollutant emitted from a type P5000 metal etcher (Applied Materials, Inc.) during preventive maintenance was investigated in this study. Sulfur hexafluoride (SF_6) gas of 1000 ppm was released at different flow rates at the bottom of the chamber to simulate the emission. When a large flow rate of 3130 L/min was vented from the venting port near the top of the chamber, the control efficiency of air pollutant is nearly 100%, whether the top of the chamber was open or enclosed with a specially-designed cover. The SF_6 concentration at the breathing zone was found to be lower than the detection limit of the FTIR spectrometer. Numerical simulation of the flow and pollutant concentration fields yielded control efficiencies in good agreement with the experimental data. When the chamber was open, the control efficiency remained at 100% if the venting flow rate was greater than 1200 L/min; while the control efficiency decreased with decreasing flow rate. In comparison, the control efficiency with the specially-designed cover, which had a much smaller opening, was 100% for venting flow rates as low as 31.3 L/min..

Keywords: Cleanroom; Pollutant dispersion; Ventilation; Indoor air pollution.

[*] Corresponding author: Tel.: +886-3-5731880, Fax: +886-3-5727835

E-*mail address*: cjtsai@mail.nctu.edu.tw

INTRODUCTION

Chlorine and boron chloride are the major process gases used in metal etchers in the semiconductor industry. In plasma etching, process gases are ionized in the reactor chamber to form free radicals, which etches off aluminum film from the wafer surface under conditions of high-energy plasma. To increase product yield, by-products deposited on the chamber wall must be cleaned periodically during preventive maintenance. During cleaning the reaction chamber is opened and its walls wiped with a cloth soaked with de-ionized water or isopropyl alcohol (IPA). Toxic gases are released which may disperse in the cleanroom, posing health threats to workers, or contaminating wafer quality and leading to defects.

The toxicity of waste gases, contaminated vacuum oils and solid debris originating from the metal etcher have been studied in acute oral and sub-chronic inhalation tests with laboratory rats by many previous investigators (Bauer *et al.*, 1992; Bauer *et al.*, 1995; Schmidt *et al.*, 1995; Bauer *et al.*, 1996; Muller *et al.*, 2002). An extractive Fourier transform infrared (FTIR) spectrometer was successfully used to locate, identify and quantify the odor sources inside the cleanroom of a semiconductor-manufacturing plant (Li *et al.*, 2003). The FTIR was used to monitor the hazardous gases emitted during preventive maintenance of a metal etcher, including HCl, HCN, CCl_4, HCOOH, CO and IPA. The peak concentrations of the above gases were found to be 195, 220, 5.4, 5.18, 5.93, and 464 ppm in the chamber, respectively (Chang *et al.*, 2000). To protect themselves, engineers have to wear full-face breathing respirators as a standard operating procedure. Therefore, it is very important to control toxic-gas release during preventive maintenance.

In open literature, SF_6 tracer gas was used to evaluate the control efficiency of an industrial local exhaust hood (Hampl, 1984; Hampl *et al.*, 1986) and laboratory fume hood (Ivany *et al.*, 1989). Numerical simulations were made to evaluate the control efficiency of the local exhaust/ventilation hood (Kulmala, 1994; Kulmala 1995a; Kulmala 1995b; Kulmala and Saarenrinne, 1996; Heinonen *et al.,* 1996; Kulmala, 2000). The use of a local ventilation hood installed with a low-vacuum cleaning line appears to effectively prevent toxic gas emission during preventive maintenance activities in a semiconductor industry cleanroom (Li *et al.*, 2005).

In this study, we further extended the experimental work to cover the case when the chamber was open, and at various release flow rates of SF_6 gas. Numerical method was further used to elucidate the differences in control efficiency due to different venting flow rates from the chamber which was either open at the top, or enclosed by a special hood designed with a hole just small enough to allow the worker’s hand to access the chamber for cleaning.

EXPERIMENTAL METHOD

The experiment incorporated the use of a type P5000 metal etcher (Applied Materials, Inc.), with a cylindrical chamber of 30.5 cm in diameter (depth: 21 cm), and a distance of 9.5 cm from the chamber opening to the center of the venting port (diameter: 5.8 cm). The top of the chamber is about 122 cm above the clean-room floor. Two cases were tested. In Case 1, shown in Fig. 1, the chamber was open at the top and the gas was vented through the venting port via a low-vacuum line (inner diameter: 3.8 cm, outer diameter: 4.5 cm, and length: 5.6 m) near the top at a large flow rate of 3130 ± 60 L/min. In Case 2, as shown in Fig. 2, the chamber was covered with an enclosed hood and vented through the same venting port at the same flow rate. On the top of the hood, a hole with a diameter of 10 cm allowed the worker to access the chamber to clean it by hand. SF_6 tracer gas of 1000 ppm was released at the bottom of the chamber through 14 small holes (diameter: 2 mm) drilled evenly on a circular 1/4" Teflon tube. The control efficiency for the hood (Case 2) was measured when the SF_6 flow rate was 5 L/min, while that without the hood (Case 1) was measured at the SF_6 flow rate of 1, 5, 8, and 10 L/min, respectively.

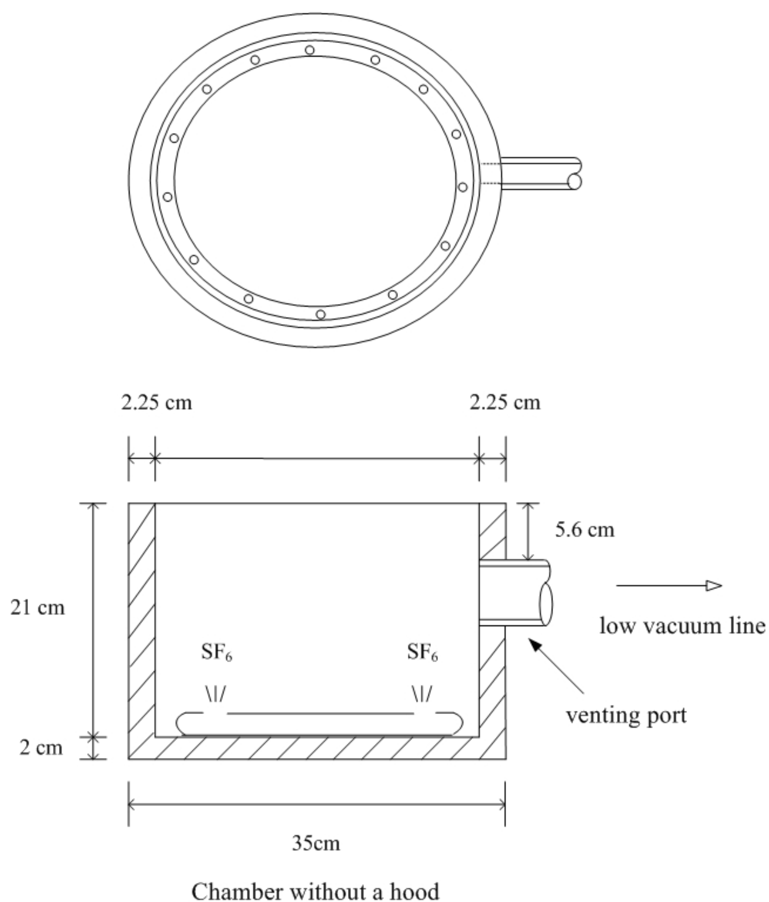

Fig. 1. Chamber configuration of a metal etcher.

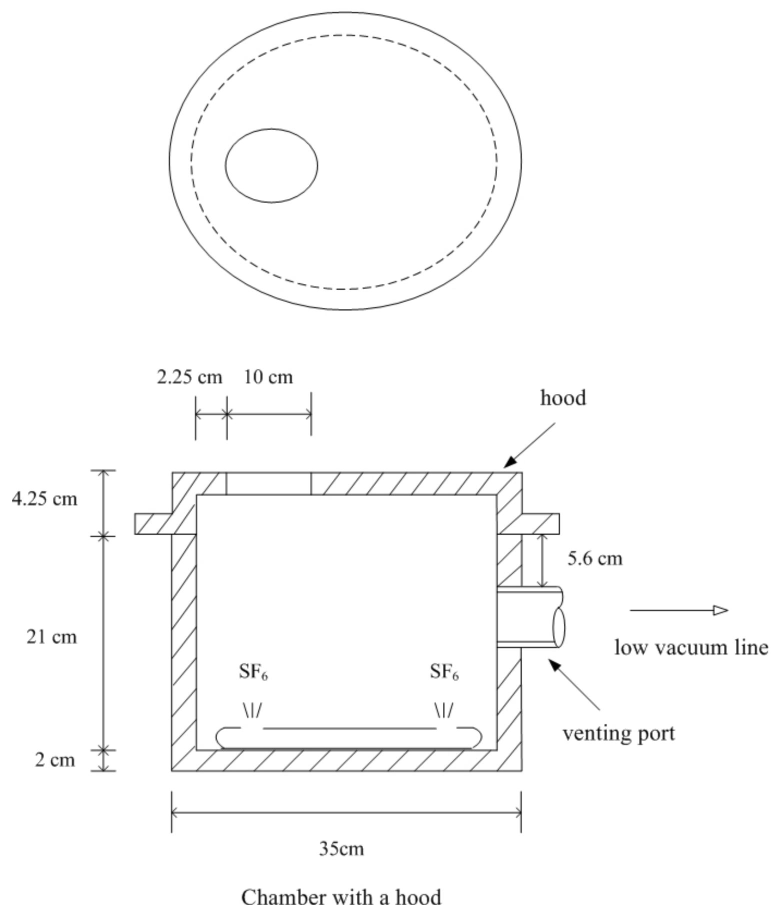

Fig. 2. Chamber configuration of a metal etcher with a specially-designed hood.

The setup for measuring the control efficiency was the same as Li *et al.* (2005) and is shown in Fig. 3. The experimental data were obtained using a Bomen FTIR (Fourier transform infrared spectrometer, ABB Bomem, Canada), which was equipped with a liquid-nitrogen detector and a gas cell (EA-2L/10m, Gemini, USA) with an optical path length of 10 m. Details of FTIR experimental procedures and configurations are described in Li *et al.* (2003). The control efficiency, *CE*, is defined as:

$$CE = \frac{C_m}{C_i} \times 100\% \tag{1}$$

where C_m is the SF_6 concentration in the low-vacuum venting tube when the tracer gas is released at the bottom of the chamber, and C_i is the SF_6 concentration in the low-vacuum venting line when the tracer gas is introduced directly into the vacuum line.

In Case 1, the airflow velocity at the chamber opening (average flow rate of air supply: 2.54 m^3/min) of the type P5000 metal etcher chamber was 0.6 m/s on average. In Case 2, the airflow velocity at the opening of the hood (average flow rate of air supply : 2.31 m^3/min) was 4.9 m/s on

average. We stretched a hand into the chamber through the access hole to simulate the wall cleaning action during preventive maintenance. At the venting flow rate of 3130 ± 60 L/min, the venting velocity through the low-vacuum venting tube was 46 ± 1 m/s. The vertical downward flow velocity of the cleanroom was 0.3 m/s. The height of the personnel breathing zone near the chamber was 150 cm from the clean-room floor.

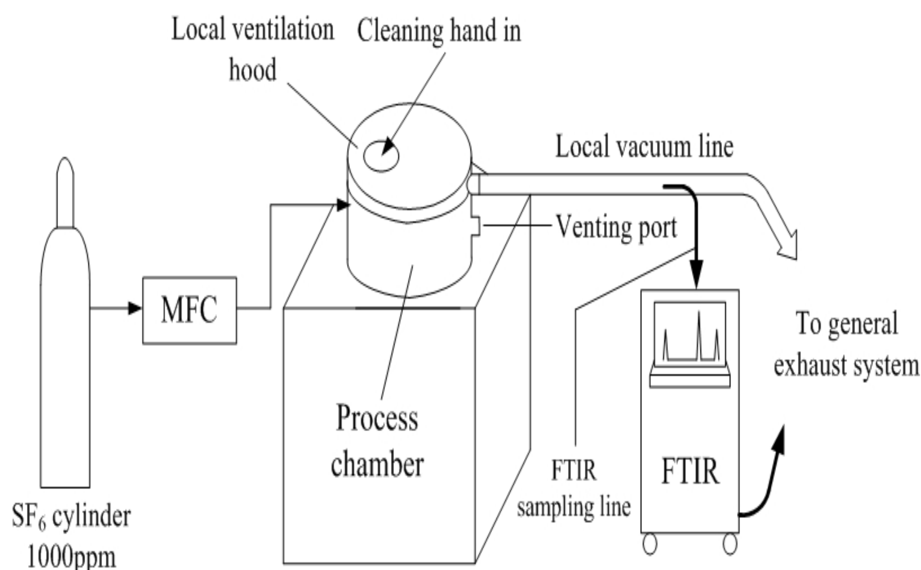

Fig. 3. Experimental setup for measuring control efficiency.

NUMERICAL METHOD

Governing equations

According to the cleanroom's airflow characteristics, steady state and incompressible flow with constant physical properties and temperature was assumed. Mass continuity equations and Reynolds-averaged Navier-Stokes equations were solved with turbulence closure provided by the standard *k*-*ε* turbulence model. The governing equations of airflow can be written as (STAR-CD Methodology, 2004):

$$\frac{\partial}{\partial x_j}\left(\rho \bar{u}_j\right)=0 \tag{2}$$

$$\frac{\partial}{\partial x_j}\left(\rho \bar{u}_j \bar{u}_i-\tau_{ij}\right)=-\frac{\partial \bar{p}}{\partial x_i} \tag{3}$$

In the above equations, the over bar denotes the ensemble averaging process. x_i is Cartesian coordinate (i = 1, 2, 3), $\bar{u}_i$ is the ensemble average velocity in direction x_i, $\bar{p}$ is the ensemble average pressure, and ρ is the mass density. τ_{ij} is stress tensor component and can be written as:

$$\tau_{ij} = 2\mu s_{ij} - \frac{2}{3}\mu\frac{\partial u_k}{\partial x_k}\delta_{ij} - \bar{\rho}\overline{u_i'u_j'} \tag{4}$$

where μ is molecular dynamic fluid viscosity and δ_{ij} is the Kronecher delta. s_{ij}, the rate of strain tensor, is given by:

$$s_{ij} = \frac{1}{2}\left(\frac{\partial u_i}{\partial x_j} + \frac{\partial u_j}{\partial x_i}\right) \tag{5}$$

The standard k-ε turbulence model was applied to model the turbulent effects in this study. The equation of turbulence kinetic energy can be written as:

$$\frac{\partial}{\partial x_j}(\rho u_j k - \frac{\mu_e}{\sigma_k}\frac{\partial k}{\partial x_j}) = \mu_t P_t - \rho\varepsilon - \frac{2}{3}(\mu_t\frac{\partial u_i}{\partial x_i} + \rho k)\frac{\partial u_i}{\partial x_i} \tag{6}$$

where μ_t, the turbulent viscosity, and μ_e, the effective viscosity, are defined as:

$$\mu_t = \frac{C_\mu \rho k^2}{\varepsilon} \tag{7}$$

$$\mu_e = \mu + \mu_t \tag{8}$$

The equation of turbulence dissipation rate is expressed as:

$$\frac{\partial}{\partial x_j}(\rho u_j \varepsilon - \frac{\mu_e}{\sigma_\varepsilon}\frac{\partial \varepsilon}{\partial x_j}) = C_{\varepsilon 1}\frac{\varepsilon}{k}\left[\mu_t P_t - \frac{2}{3}(\mu_t\frac{\partial u_i}{\partial x_i} + \rho k)\frac{\partial u_i}{\partial x_i}\right] - C_{\varepsilon 2}\rho\frac{\varepsilon^2}{k} - C_{\varepsilon 3}\rho\varepsilon\frac{\partial u_i}{\partial x_i} \tag{9}$$

where C_μ, $C_{\varepsilon 1}$, $C_{\varepsilon 2}$, $C_{\varepsilon 3}$, σ_k, σ_ε, are empirical coefficients whose values are:

$C_\mu = 0.09$, $C_{\varepsilon 1} = 1.44$, $C_{\varepsilon 2} = 1.92$, $C_{\varepsilon 3} = 0.33$, $\sigma_k = 1.0$, and $\sigma_\varepsilon = 1.22$.

CFD model

In the calculation domain, multi-blocked tetragon grids were generated by using an automatic mesh generation tool, Pro-Modeler 2003 (CD-Adapco Japan Co., LTD). The computational domain is 2m x 2m x 3m (393,000 grids), as shown in Fig. 4. The maximum and minimum length of the mesh are 10 cm and 0.02 cm, respectively. The accuracy of the simulation was checked by using different numbers of grids. It was found that increasing from 393,000 to 810,000 grids only resulted in a less than 0.1% difference in the control efficiency. Therefore, to save computation time, 393,000 grids were used for all calculations in this study.

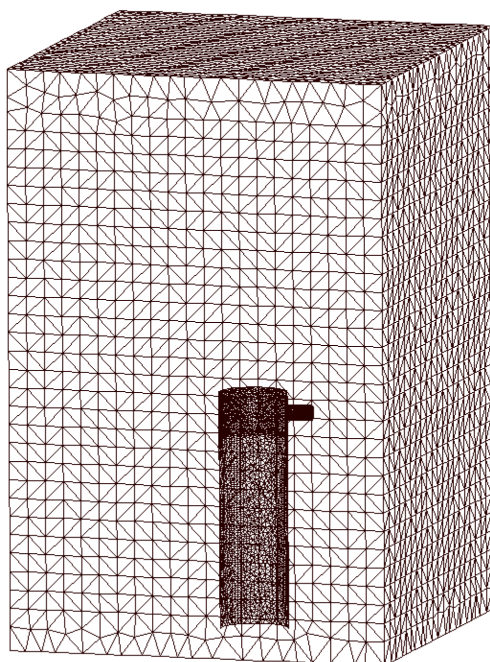

Fig. 4. Calculation domain and grids.

The differential equations governing the conservation of mass, momentum, and energy were solved by STAR-CD 3.22 code (CD-Adapco Japan Co., LTD), which is based on the finite volume discretization method. In the code, the estimation of diffusion fluxes at cell faces is obtained by a centered approximation, while upwind differencing is adopted for the convective fluxes. The pressure-velocity linkage is solved by the SIMPLE (semi-implicit method for pressure linked equation) algorithm (Patankar *et al.*, 1972). Turbulence intensity was assumed to be 10%, and turbulence length scale was assumed to be 0.1 times the diameter of the opening of the distribution tube. The convergence criterion of the flow field calculation was set to 0.001 for the summation of the residuals. The computations required 2.5 hours of CPU time on a computer with an Intel Pentium 4 processor at 3.0 GHz.

In the simulation, the boundary conditions were set as follows. For the release of pollutant source at the bottom of the chamber, SF_6 was solved as a scalar species in dispersion calculation.

In Fig. 4, a uniform, downward airflow of 0.3 m/s was assigned at the top boundary of the domain. The other 5 boundaries of the computational domain were assigned as pressure boundaries to meet the mass conservation requirement. With the STAR-CD, local injection/extraction can be used anywhere within the mesh. The injection/extraction process was modeled as an additional source/sink term s_φ in the finite volume equation. The term is of the form:

$$s_\varphi = \dot{m}\varphi \tag{10}$$

where $\dot{m}$ is the mass flow rate of the injected/extracted stream per unit volume, and φ stands for any of the dependent variables.

In order to simulate venting at the venting port, the mass sink was calculated by a user subroutine which specified the mass fluxes removed at specified grids. At the low vacuum line, the sink region was assumed with a thickness of 0.3 cm in the fluid. The mass flow rate of sink, $\dot{m}_{\sin k}$, can be calculated as:

$$\dot{m}_{\sin k} = -\frac{\rho_{air} \times U_d \times A}{\overline{V_d}} = -\rho_{air} \times \frac{Q}{\overline{V_d}} \tag{11}$$

where ρ_{air} is the air density, U_d is the venting velocity, A is the cross section area, Q is the venting flow rate, and $\overline{V_d}$ is the removal volume.

To simulate the wiping of the chamber wall during preventive maintenance, a rotating reference frames method was applied to the chamber with the special cover. The rotating reference frames method enables one to model the case where the entire mesh is rotating at a constant angular velocity. The modeling strategy dictated that the mesh of fluid inside the chamber be assigned to the rotating frame to make the fluid rotate, and changing the local coordinate systems from the Cartesian to the cylindrical system at the center of the chamber bottom. All of the fluid inside the chamber was made to rotate at an angular velocity of 5 rpm around a prescribed axis.

Control efficiency

The predicted control efficiency, *CE*, can be written as:

$$CE = \frac{\dot{m}_{out}}{\dot{m}_{in}} \times 100\% \tag{12}$$

Where,

$$\dot{m}_{out} = \sum Y_{out} \times Q_{out} \times \rho_{air} \quad (13)$$

$$\dot{m}_{in} = \left[Y_{in}\right]_{kg/m^3} \times Q_{in} \quad (14)$$

where $\dot{m}_{in}$ and $\dot{m}_{out}$ are the SF_6 mass flow rate at the bottom of the chamber and the SF_6 mass flow rate at the low-vacuum line, respectively. Q_{in} and Q_{out} are the inlet flow rate and the outlet flow rate, respectively. $\left[Y_{in}\right]_{kg/m^3}$ and Y_{out} are the SF_6 mass concentration at the inlet in kg/m^3 and the SF_6 mass fraction at the outlet, respectively.

For Cases 1 and 2, different SF_6 release flow rates (1, 5, 8 and 10 L/min) and side venting flow rates (0, 31.3, 93.9, 156.5, 313, 1565, 3130 and 4695 L/min) were simulated. The control efficiencies of side venting at different flow rates were investigated by changing the mass sink in the simulation.

RESULTS AND DISCUSSIONS

Case 1–Chamber is open at the top

The results of flow and concentration fields and the comparison of the experimental control efficiencies and simulated values are presented here for Case 1 at the large venting flow rate of 3130 L/min. For example, Fig. 5(a) shows the airflow field when SF_6 is released at the flow rate of 10 L/min, and the side venting flow rate is at the maximum of 3130 L/min, at the vertical cross-section plane of the chamber. Upward injected SF_6 flow at the opening of the gas distribution tubes can be observed at the bottom of the chamber. Both airflows inside the chamber and near the chamber top are seen to be sucked completely into the venting port. There is no outward SF_6 flow at the top of the chamber. The corresponding SF_6 concentration field is shown in Fig. 5(b). It is observed that with the large venting flow rate of 3130 L/min, the SF_6 concentration near the top of the chamber is about zero, meaning there is no observable SF_6 outflow from the chamber. The results are consistent with the flow field seen in Fig. 5(a).

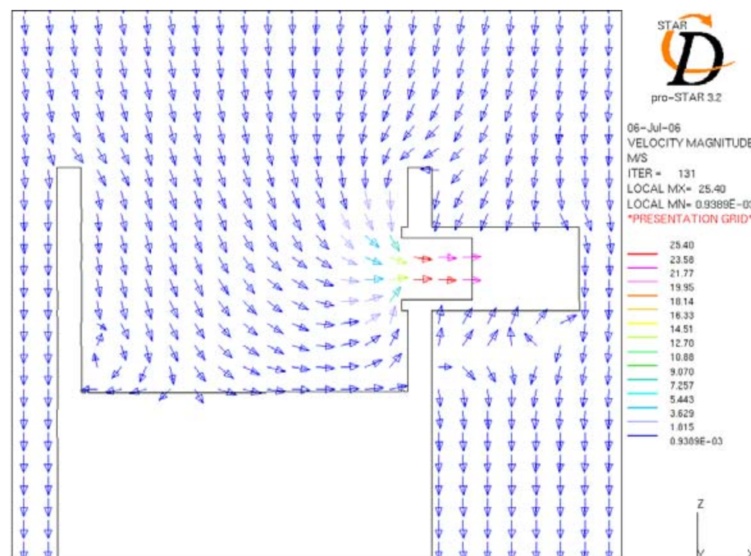

Fig. 5(a). Velocity vectors for SF_6 release flow rate of 10 L/min, venting flow rate of 3130 L/min, Case 1.

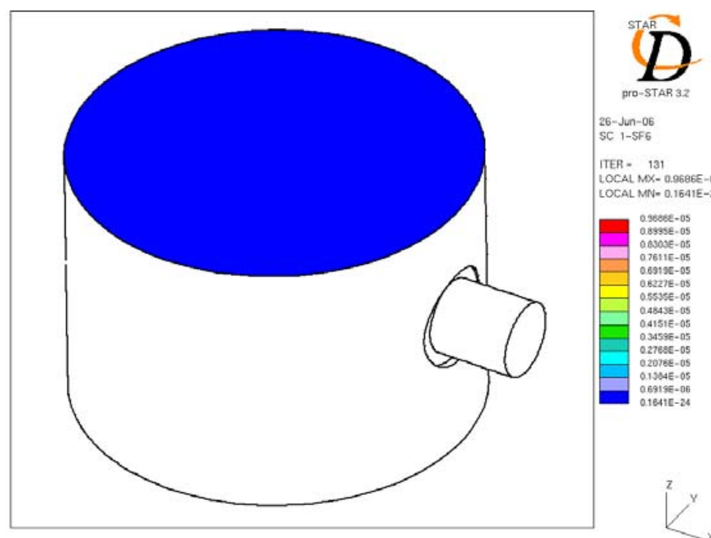

Fig. 5(b). Concentration field for SF_6 release flow rate of 10 L/min, venting flow rate of 3130 L/min (Case 1).

Table 1 is the summary of the experimental data when the side venting flow rate is 3130 L/min. As listed in Table 1, the control efficiency by side venting without the hood (Case 1) is 95.5%, 97.8%, 98.3%, and 98.0% for the SF_6 release flow rate of 1, 5, 8, and 10 L/min, respectively. The experimental control efficiencies stand in high values, but tend to increase as SF_6 release flow rate increases. The error source may come from gas-phase infrared spectral standards provided by the FTIR manufacturer. As shown in Fig. 6, the simulated results compare well with the experimental data, indicating that the modeling method is accurate.

Table 1. Experimental data under different conditions when the side venting flow rate is 3130 L/min.

SF_6 flow rate (L/min)	Case	SF_6 concentration at breathing zone (ppm)	SF_6 concentration[a] (ppm)	SF_6 concentration[b] (ppm)	Control efficiency (%)
5	2	N.D.	0.78	0.80	97.5
5	2	N.D.	0.81	0.82	98.8
1	1	N.D.	0.21	0.22	95.5
5	1	N.D.	0.88	0.90	97.8
8	1	N.D.	1.18	1.20	98.3
10	1	N.D.	1.46	1.49	98.0

It is necessary to look into the personnel exposure at the breathing zone after utilizing the side venting method for a fully open chamber. As shown in Fig. 7, there is no observable SF_6 concentration at the breathing zone when SF_6 is released at the flow rate of 10 L/min, and the venting flow rate is at a maximum of 3130 L/min. In Table 1, the experimental results of Case 1 also show that SF_6 concentration at the breathing zone is lower than FTIR detection limit of 5 ppb at different SF_6 release flow rates. Simulated SF_6 concentration at the breathing zone is also nearly zero.

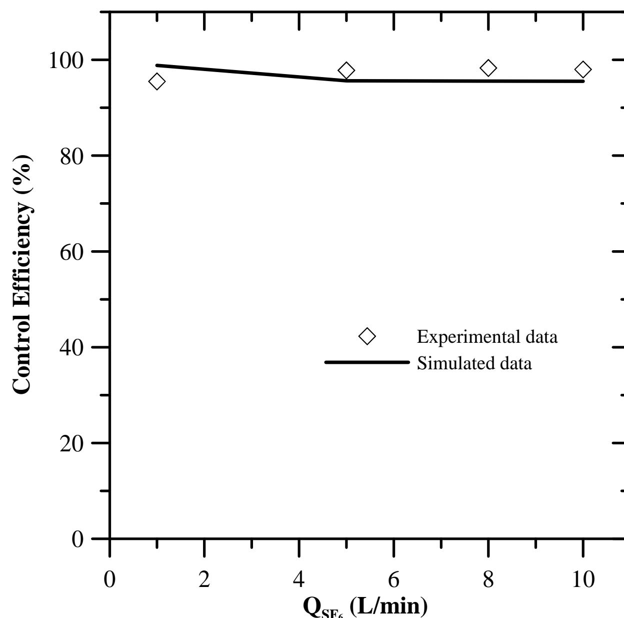

Fig. 6. Measured and simulated control efficiency versus SF_6 flow rate when the side venting flow rate is 3130 L/min (Case 1).

Fig. 7. Concentration field around the chamber and at the breathing zone for SF_6 release flow rate of 10 L/min, venting flow rate of 3130 L/min (Case 1).

Case 2–Chamber is enclosed by the hood

The results of flow and concentration fields and the comparison of the experimental control efficiencies and simulated values are presented here for Case 2 at the large venting flow rate of 3130 L/min. For example, Fig. 8(a) shows the airflow field for the chamber with the enclosed hood when SF_6 is released at the flow rate of 10 L/min, and the venting flow rate is at 3130 L/min. It can be observed that downward airflow enters the chamber through the small opening of the hood, then airflow re-circulating upward inside the chamber is confined by the hood. Both airflows inside the chamber and near the chamber top are seen to be sucked into the venting port more completely than in Case 1; and there is no outward SF_6 flow at the opening of the hood.

The concentration field of SF_6 at the release flow rate of 10 L/min, and the venting flow rate of 3130 L/min (100%) is shown in Fig. 8(b). It is observed that when there is an enclosed hood at the top of the chamber, the SF_6 concentration near the opening of the hood is about zero, meaning there is no observable SF_6 outflow through the opening of the hood.

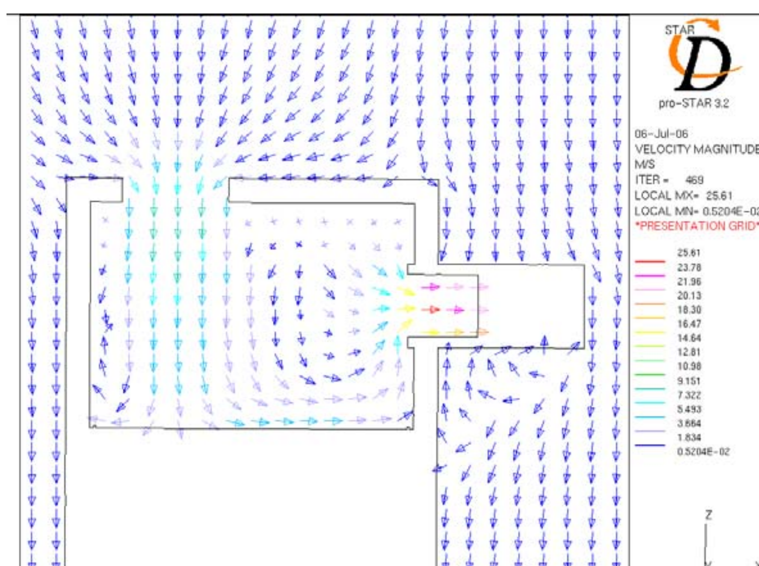

Fig. 8(a). Velocity vectors of the chamber with the hood for SF_6 release flow rate of 10 L/min, venting flow rate of 3130 L/min (Case 2).

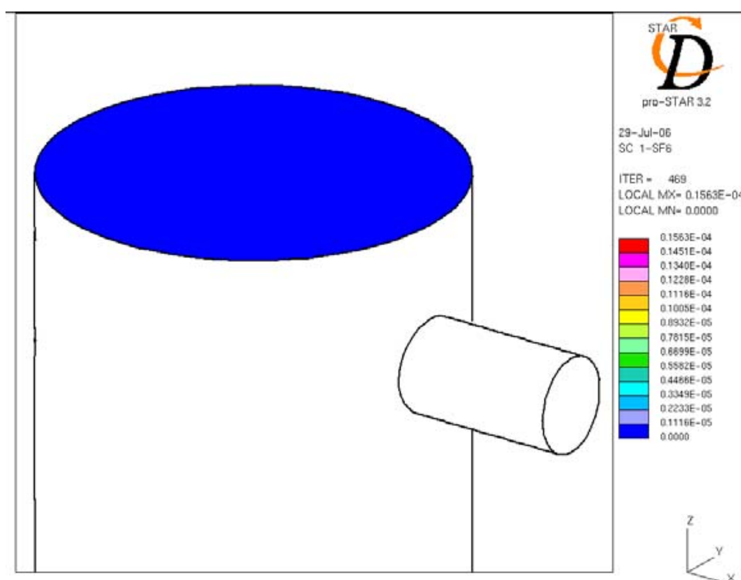

Fig. 8(b). Concentration field of the chamber with the hood for SF_6 release flow rate of 10 L/min, venting flow rate of 3130 L/min (Case 2).

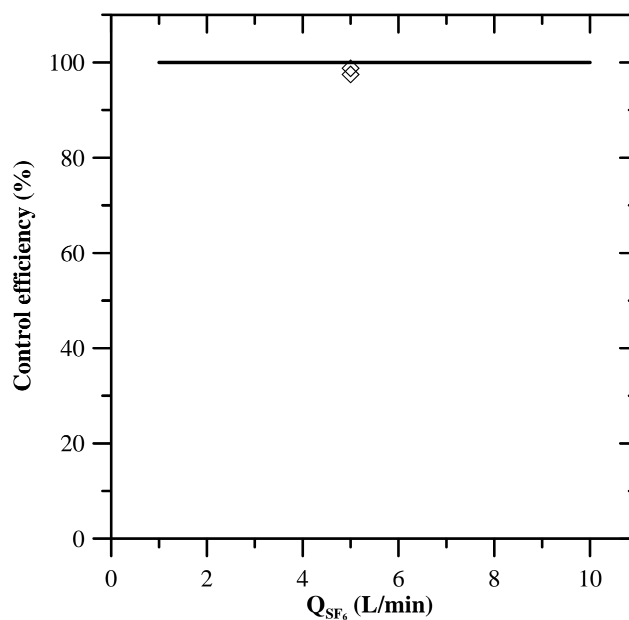

Fig. 9. Measured and simulated control efficiency of SF_6 versus total gas flow rate when the side venting flow rate is 3130 L/min (Case 2).

The measured and simulated control efficiency of SF_6 versus total gas flow rate when the side venting flow rate is 3130 L/min is shown in Fig. 9. The simulated control efficiency is 100% at the SF_6 release flow rate of 1, 5, 8, and 10 L/min. The measured control efficiency is 97.5% or 98.8% when the SF_6 release flow rate is 5 L/min (also listed in Table 1). The experimental SF_6 concentration at the breathing zone is lower than FTIR detection limit (< 5 ppb) when the SF_6 release flow rate is 5 L/min and the venting flow rate is 3130 L/min. Simulated SF_6 concentration at the breathing zone also approaches to zero.

Effect of different venting flow rates on the control efficiency

In order to investigate the effect of different venting flow rates on the control efficiency, different venting flow rates (0, 31.3, 93.9, 156.5, 313, 1565, 3130 and 4695 L/min) were simulated at a fixed SF_6 release flow rate of 10 L/min. For example, in Case 1, when the venting flow rate is reduced to 10% of the maximum value, or 313 L/min, the flow field is changed completely, as shown in Fig. 10(a). The flow near the venting port still converges with it while some of the flow at the far end of the venting port escapes the chamber top, leading to SF_6 potentially leaking into the cleanroom. The concentration field of SF_6 shown in Fig. 10(b) indicates either that significant SF_6 concentration exists at the top of the chamber, or that SF_6 is leaking from the chamber. These results are consistent with the flow field seen in Fig. 10(a).

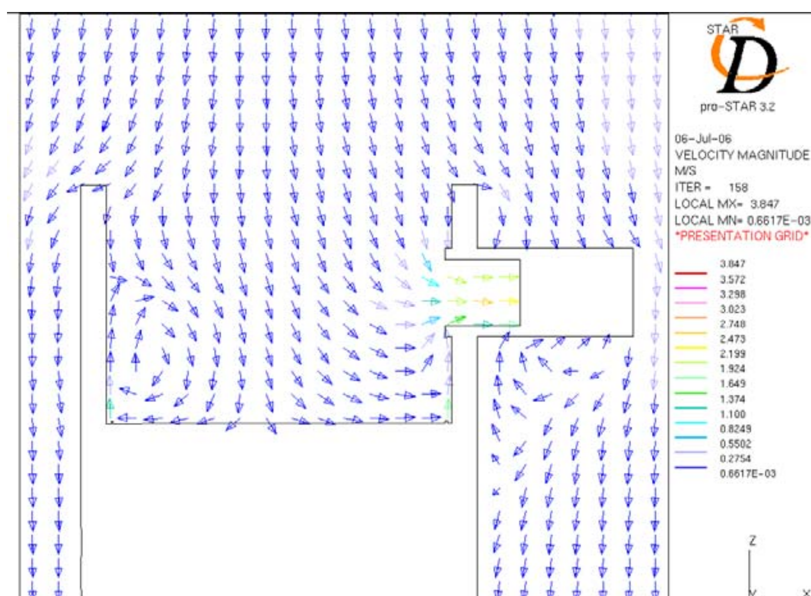

Fig. 10(a). Velocity vectors for SF_6 release flow rate of 10 L/min, venting flow rate of 313 L/min (Case 1).

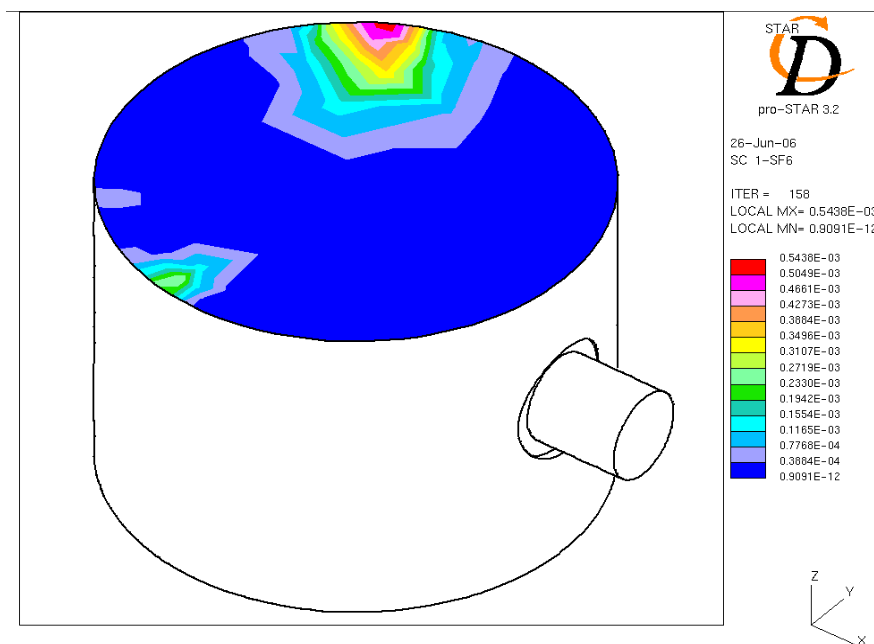

Fig. 10(b). Concentration field for SF_6 release flow rate of 10 L/min, venting flow rate of 313 L/min (Case 1).

Table 2 shows the simulated control efficiency when the side venting flow rate is 313 L/min for Case 1. The control efficiency is 81.9%, 72.7%, 74.7% and 73.5% at the SF_6 release flow rate of 1, 5, 8, and 10 L/min, respectively. These results are consistent with the flow and concentration fields seen in Fig. 10 showing that SF_6 concentration exists at the top of the chamber when the side venting flow rate is reduced to 313 L/min. Simulated SF_6 concentration at the breathing zone is also lower than the FTIR detection limit. However, the simulated control efficiency at the SF_6 release flow rate of 5 L/min is less than that of 8 L/min. This is due to the simplification of the calculation for obtaining the simulated control efficiency that requires considering the contribution by convection and diffusion.

Table 2. Simulated control efficiency when the side venting flow rate is 313 L/min (Case 1).

Calculation domain (X* Y* Z)	SF_6 release flow rate (L/min)	Simulated control efficiency (%)
2m* 2m* 3m	1	81.9
	5	72.7
	8	74.7
	10	73.5

Fig. 11 shows the effect of venting flow rate on the control efficiency for Case 1, when the SF_6 release rate is fixed at 10 L/min. When the venting flow rate is higher than 1200 L/min, the control efficiency is found to be nearly 100% higher and becomes more or less a constant. Below 1200 L/min, the control efficiency drops sharply. A similar trend also occurs for SF_6 release flow rates of 8, 5, and 1 L/min. The results show that side venting at a large flow rate should be an effective way to control pollutant dispersion, thus reducing the worker's exposure during preventive maintenance.

In Case 2, as described in the previous section, simulated control efficiency is 100% at the SF_6 release flow rate of 1, 5, 8, and 10 L/min, when the side venting flow rate is at the maximum value of 3130 L/min. When the venting flow rate is reduced to 10% of the maximum value (or 313 L/min), the flow and concentration fields are similar to the results of the venting flow rate at 3130 L/min. The flow near the venting port is still converged into it and the SF_6 concentration near the opening of the hood is about zero, meaning there is also no observable SF_6 outflow through the small opening of the hood. At this venting flow rate, the simulated control efficiency is 100% at the SF_6 release flow rate of 1, 5, 8, and 10 L/min. Further simulation shows that the control efficiency with the specially-designed cover remains 100% for a venting flow rate of as low as 31.3 L/min, due to the much smaller opening. Such a flow rate is much smaller than that required in Case 1.

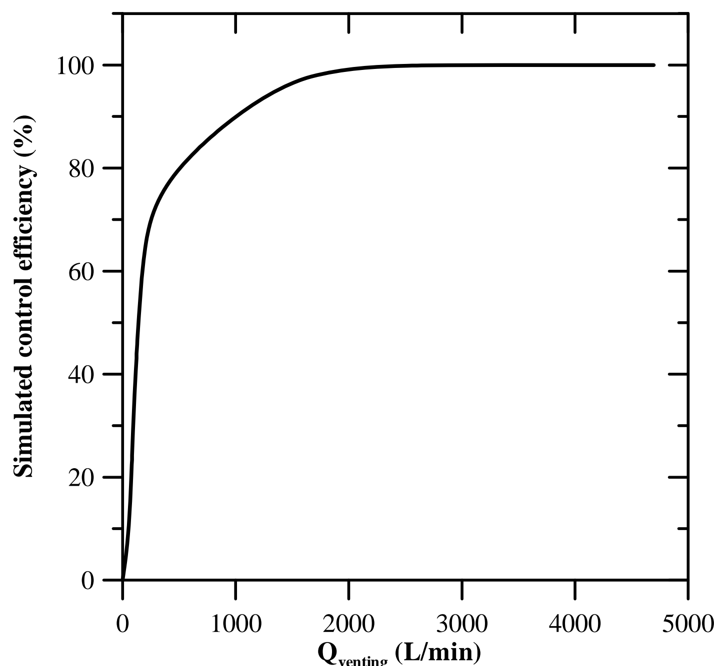

Fig. 11. Simulated control efficiency of SF_6 versus different side venting flow rates when SF_6 release flow rate is 10 L/min (Case 1).

Therefore, it can be concluded that a high degree of control of pollutant dispersion can be achieved to effectively protect the worker from exposure by installing the hood and using side venting at a reasonable flow rate during preventive maintenance.

CONCLUSION

This study presents the numerical results and experimental data for the control efficiency of air pollutant during preventive maintenance of a metal etcher by cleaning the chamber without (Case 1) and with (Case 2) a special hood on top, and by side venting at a large flow rate. SF_6 gas was used to simulate air pollutant release in the chamber. The control efficiency of side venting at different flow rates was also investigated. Results show that pollutant dispersion of a metal dry etcher during preventive maintenance can be effectively controlled by side venting at a large flow rate near the chamber top whether the chamber is fully open (without the hood) or with a hood. Good agreement between the experimental data and the simulation results was obtained. The SF_6 concentration at the breathing zone was also found to be lower than the detection limit of the FTIR. When the side venting flow rate is reduced, but maintained above a certain value, the pollutant dispersion can still be controlled effectively, and the control efficiency of the chamber with the hood is superior to that without the hood.

The results indicate that computational fluid dynamic is a useful tool for simulating the control efficiency of a local ventilation system during preventive maintenance. It can further be used with more experimental data to design and optimize the system.

Nomenclature

C	concentration
CE	control efficiency
δ_{ij}	Kronecher delta
$\dot{m}$	mass flow rate of the injected/extracted stream per unit volume
$\dot{m}_{in}$	mass flow rate of inlet at the bottom of the chamber
$\dot{m}_{out}$	mass flow rate of outlet at the low vacuum line
$\dot{m}_{\sin k}$	mass flow rate of sink
μ	molecular dynamic fluid viscosity
μ_e	effective viscosity
μ_t	turbulent viscosity
P	sub-layer resistance factor
$\overline{p}$	ensemble average pressure
ρ	density
ρ_{air}	air density

Q	venting flow rate
Q_{in}	inlet flow rate
Q_{out}	outlet flow rate
s_{ij}	rate of strain tensor
s_{φ}	associated source coefficient
τ_{ij}	stress tensor component
U_d	venting velocity
u	fluid velocity vector
$\overline{u}_i$	ensemble average velocity in direction
$\overline{V}_d$	removal volume
x_i	Cartesian coordinate
φ	dependent variables
Y	mass fraction of species
$\left[Y_{in}\right]_{kg/m^3}$	mass concentration of species at the inlet in kg/m^3

ACKNOWLEDGMENT

The authors would like to thank the Industrial Technology Research Institute (ITRI) in Taiwan for financial support of this project in 2004.

REFERENCES

Bauer, S., Werner, N., Wolff, I., Damme, B., Oemus, K. and Hoffmann, P. (1992). Toxicological Investigation in the Semiconductor in Dustry: II Studies on the Subacute Inhalation Toxicity and Genotoxicity of Gaseous Waste Products from the Aluminium Plasma Etching Process. *Toxicol. Ind. Health.* 8: 431-444.

Bauer, S., Wolff, I., Werner, N., Schmidt, R., Blume, R. and Pelzing, M. (1995). Toxicological Investigation in the Semiconductor Industry: IV Studies on the Subchronic Oral Toxicity and Genotoxicity of Vacuum Pump Oil Contaminated by Waste Products from Aluminum Plasma Etching Processes. *Toxicol. Ind. Health.* 11: 523-541.

Bauer, S., Wolff, I., Schmidt, R. and Pelzing, M. (1996). Toxicological Hazards of Plasma Etching Waste Products. *Solid State Tech.* 39: 97-110.

Chang, C.P., Song, L.Y., Chu, C.Q. and Lin, Y.C. (2000). The Evaluation of Hazardous Gases Emission from the Preventive Maintenance Procedure in Semiconductor Factory. *IOSH (Taiwan) Quarterly.* 8**:** 205-216 (in Chinese).

Computational Dynamic Limited (2004). *STAR-CD Version 3.22 Methodology*, Computational Dynamic Limited.

Hampl, V. (1984). Evaluation of Industrial Exhaust Hood Efficiency by a Tracer Gas Technique. *Am. Ind. Hyg. Assoc. J.* 45: 485-490.

Hampl, V., Niemela, R., Shulman, S. and Bartley, D.L. (1986). Use of Tracer for Industrial Exhaust Hood Efficiency Evaluation – Where to Sample. *Am. Ind. Hyg. Assoc. J.* 47: 281-287.

Heinonen, K., Kulmala, I. and Saamamen, A. (1996). Local Ventilation for Powder Handling-Combination of Local Supply and Exhaust Air. *Am. Ind. Hyg. Assoc. J* 57: 356-364.

Ivany, R.E., First, M.W. and Diberardinis L.J. (1989). A New Method for Quantitative, In - Use testing of laboratory fume hoods. *Am. Ind. Hyg. Assoc. J.* 50: 275-280.

Kulmala, I. (1994). Numerical Simulation of a Local Ventilation Unit. *Ann. Occup. Hyg.* 38: 337-349.

Kulmala, I. (1995a). Numerical Simulation of the Capture Efficiency of an Unflanged Rectangular Exhaust Opening in a Coaxial Airflow. *Ann. Occup. Hyg.* 39: 21-33.

Kulmala, I. (1995b). Numerical Simulation of Unflanged Rectangular Exhaust Openings. *Am. Ind. Hyg. Assoc. J.* 56: 1099-1106.

Kulmala, I. and Saarenrinne, P. (1996). Air Flow Near an Unflanged Rectangular Exhaust Opening. *Energy and Buildings.* 24: 133-136.

Kulmala, I. (2000). Experimental Validation of Potential and Turbulent Flow Models for a Two - Dimensional Jet Enhanced Exhaust Hood. *Ann. Occup. Hyg.* 61: 183-191.

Li, S.N., Chang, C.T., Shih, H.Y., Tang, A., Li, A. and Chen, Y.Y. (2003). Using an Extractive Fourier Transform Iinfrared Spectrometer for Improving Cleanroom Air Quality in a Semiconductor Manufacturing Plant. *Am. Ind. Hyg. Assoc. J.* 64: 408-414.

Li, S.N., Shih, H.Y., Wang, K.S., Hsieh, K., Chen, Y.Y., Chen, Y.Y. and Chou, J. (2005). Preventive Maintenance Measures for Contamination Control. *Solid State Tech.* 48: 53-56.

Muller, P., Stock, T., Bauer, S. and Wolff, I. (2002). Genotoxicological Characterization of Complex Mixtures Genotoxic Effects of a Complex Mixture of Perhalogenated Hydrocarbons. *Mutation Res. Genetic Toxicol. Environ. Mutagenesis.* 515: 99-109.

Patankar, S.V. and Spalding, D.B. (1972). A Calculation Procedure for Heat, Mass and Momentum Transfer in Three - Dimensional Parabolic Flows, *Int. J. Heat Mass Transfer.* 15: 1787-1806.

Schmidt, R., Scheufler, H., Bauer, S., Wolff, L., Pelzing, M. and Herzschuh, R. (1995). Toxicological Investigation in the Semiconductor Industry: III Studies on Prenatal Toxicity Caused by Waste Products from Aluminum Plasma Etching Processes. *Toxicol. Ind. Health.* 11: 49-61.

Received for review, January 28, 2007
Accepted, May 31, 2007